F. ATDM simulations by TT members

F-1. The NOAA ATDM experiments[1]

The calculation of the transport and dispersion from the source was done using the Hybrid Single-Particle Lagrangian Integrated Trajectory (HYSPLIT – Draxler and Hess, 1998) model. A detailed description of the computational aspects of the model can be found in Draxler and Hess (1997) and its configuration is reviewed in the User's Guide (Draxler, 1999).

The special extract of the NOAA GDAS meteorological data archive used for the HYSPLIT ATDM calculations was available on the native hybrid sigma levels. Approximately 15 levels occur below 850 hPa with the remainder extending up to approximately 10 hPa. The three dimensional fields included the horizontal winds, temperature, and humidity. When using the GDAS data for calculations, vertical velocities were computed in HYSPLIT by integrating the divergence. The other fields used in the calculations include the surface heat and momentum fluxes for the computation of vertical mixing, the boundary layer depth, and the precipitation rate.

The ECMWF data fields had a comparable number of data fields and vertical resolution to the GDAS but included the vertical velocity field.

When using the JMA mesoscale analysis, a minimum amount of pre-processing was applied to the data which contained pressure, potential temperature, horizontal winds, moisture, and vertical velocity. The 3D pressure fields was used directly to map the data at each level to the HYSPLIT vertical sigma coordinate, potential temperature was converted to ambient temperature, and the vertical velocities were remapped to a terrain following coordinate system consistent with the HYSPLIT computational framework. A vertical velocity correction,

$$\sigma (u\, \partial\eta/\partial x + v\, \partial\eta/\partial y) \qquad \text{(F-1-1)}$$

was applied at all levels based upon the slope of the terrain surface (η) and decreasing with height (σ). With respect to the wet deposition, HYSPLIT calculations used the precipitation fields without adjustment: the MESO analysis 3-hour accumulated precipitation and calculations with the RAP used the precipitation at the grid point nearest in space (~ 1 km) and time (~ 30 min) to each particle at each integration time step.

In HYSPLIT, scavenging is parameterized through removal constants β (s^{-1}), where the deposition D over time step Δt for each particle of mass M is

$$D = M \{1-\exp[-\Delta t (\beta_{dry}+\beta_{gas}+\beta_{inc}+\beta_{bel})] \}. \qquad \text{(F-1-2)}$$

The particle mass is reduced by D each time step. The time constant for within-cloud removal for particulate pollutants is

$$\beta_{inc} = S\, P\, \Delta Z_p^{-1}, \qquad \text{(F-1-3)}$$

[1] R. Draxler

where S is the ratio of the pollutant's concentration in water to its concentration in air ($4x10^4$), ΔZ_p is the depth of the pollutant layer, and the precipitation rate P is the value predicted by the meteorological model used in the calculation. Below-cloud removal is defined directly as a rate constant ($\beta_{bel} = 5x10^{-6}$), independent of the precipitation rate. The wet deposition of gases depends upon their solubility and for inert non-reactive gases it is a function of the Henry's Law constant (H - Molar atm^{-1}), the ratio of the pollutant's equilibrium concentration in water to that in air. Therefore, the gaseous wet removal time constant is

$$\beta_{gas} = H\ R\ T\ P\ \Delta Z_p^{-1}, \qquad \text{(F-1-4)}$$

where R is the universal gas constant (0.082 atm $M^{-1}\ K^{-1}$), T is temperature, and the wet removal of gases is applied at all levels from the ground to the top of the cloud-layer. The dry deposition calculation is limited to particles within the surface layer (ΔZ_s is usually about 75 m), and the time constant is

$$\beta_{dry} = V_d\ \Delta Z_s^{-1}. \qquad \text{(F-1-5)}$$

One critical aspect for quantitative predictions of air concentration is the wet and dry scavenging that occurs along the transport pathway. Three generic species were tracked as surrogates for the radionuclides: a gas with no wet or dry scavenging, a gas with a relatively large dry deposition velocity (0.01 m/s) and wet removal (Henry's constant = 0.08) to represent gaseous I^{131}, and a particle with a small deposition velocity (0.001 m/s). There can be considerable variability in scavenging coefficients and the wet scavenging coefficients used in these calculations are lower than the original model default values (Draxler and Hess, 1997) but these lower values are consistent with the results from more recent deposition studies using the HYSPLIT scavenging parameterizations.

F-2. The Met Office ATDM Experiments[1]

NAME (Numerical Atmospheric-dispersion Modelling Environment) is the UK Met Office's Lagrangian particle dispersion model and it is used to model the atmospheric transport and dispersion of a range of gases and particles (Maryon et al., 1999 and Jones et al. 2007). It was originally developed to model the transport of radioactive material following the Chernobyl accident but now has a wide range of applications including simulating releases of hazardous materials (chemical, biological, radiological and nuclear) (Leadbetter et al 2013, Draxler et al 2012, Becker et al 2007, Ryall and Maryon 1998), modelling the transport of ash clouds from volcanic eruptions (Webster 2012), modelling the airborne transmission of diseases (Burgin 2012), forecasting air quality, analyzing air pollution episodes and identifying source locations and source strengths.

In NAME, large numbers of model particles are released into the model atmosphere, where each particle represents a certain mass of the material (gases or aerosols) being released. These particles are advected within the model atmosphere by input three-dimensional winds from numerical weather prediction models and turbulent dispersion is simulated by random walk techniques; particle velocities are correlated in time at short ranges while the more simple Wiener process is applied for longer range problems. Gravitational settling of particles and loss processes, such as wet and dry deposition, radioactive decay, cloud gamma (Bedwell 2011) and chemical transformations, are calculated when required.

NAME is typically run using NWP data from the Met Office or ECMWF but can be configured to use data in GRIB format from any model provided a suitable variable set is available. In addition, NAME can use radar rainfall observations in place of NWP rainfall estimates. NAME can use both limited area and global deterministic data as well as ensemble data (through an in-built ensemble framework). These NWP data sets can be nested both in space and time.

For the WMO Task Team work NAME was run with Met Office, ECMWF and JMA Mesoscale NWP with and without JMA Radar Rainfall observations sample deposition results for ^{137}CS are shown in Figure F-2-1. In order to use the JMA Mesoscale data it was necessary to pre-process the data to reformat it into a coordinate system supported by NAME and also to generate a number of additional fields required by NAME: converting potential temperature to temperature, converting accumulated rainfall to mean rates, estimating cloud cover, boundary layer depth and the estimation of surface fluxes of heat and momentum. Surface roughness was also absent and values from ECMWF were used in their place.

Dry deposition is modelled in NAME using the concept of the deposition velocity, v_d (Webster and Thomson, 2011). The flux of pollutant to the ground, F, is proportional to the concentration, C, of pollutant and is given by

$$F = v_d C \qquad \text{(F-2-1)}$$

[1] M. C. Hort and S. J. Leadbetter

where v_d is the constant of proportionality. The deposition velocity can either be specified by the user, which was the case for all the calculations discussed in this report, or is calculated using a resistance analogy

$$v_d = \frac{1}{R_a + R_b + R_c}, \qquad \text{(F-2-2)}$$

where R_a is the aerodynamic resistance, R_b is the laminar layer resistance and R_c is the surface resistance. The aerodynamic resistance represents the efficiency with which material is transported to the ground by turbulence and is independent of the material. The laminar layer resistance is used to specify the resistance to transport by diffusion across the thin quasi-laminar layer adjacent to the surface. Different parameterizations for R_b are used for gases and particles. The surface resistance characterizes the resistance to capture by the surface and is dependent on both the pollutant and the underlying surface. For particles, the surface resistance is taken to be zero. For gases, a fixed surface resistance can be specified by the user or, for a selection of gases, a complex land use dependent surface resistance parameterization can be invoked.

The removal of material from the atmosphere by wet deposition is based on the depletion equation

$$\frac{dC}{dt} = \Lambda C \qquad \text{(F-2-3)}$$

where C is the air concentration and Λ is the scavenging coefficient. The scavenging coefficient is given by

$$\Lambda = Ar^B \qquad \text{(F-2-4)}$$

where r is the rainfall rate (in mm hr^{-1}) and A and B are coefficients which vary for different types of precipitation (i.e., large-scale/convective and rain/snow) and for different wet deposition processes (i.e., rainout, washout and the seeder-feeder process) (see Table F-2-1) (Maryon et al., 1999). Within NAME, wet deposition due to convective and large-scale precipitation are computed separately and summed to give total wet deposition. Material located above the cloud top is not subject to wet deposition. Enhanced wet deposition (due to the seeder-feeder process) is applied to material close to the ground in regions of elevated orography.

Table F-2-1. Scavenging coefficients used in NAME

	Rain		Snow/Ice	
	Large-Scale	Convective	Large-Scale	Convective
Orographic enhancement (seeder-feeder)	$A = 3.36 \times 10^{-4}$ $B = 0.79$	$A = 3.36 \times 10^{-4}$ $B = 0.79$	$A = 1.0 \times 10^{-3}$ $B = 0.79$	$A = 1.0 \times 10^{-3}$ $B = 0.79$
Below-cloud (washout)	$A = 8.4 \times 10^{-5}$ $B = 0.79$	$A = 8.4 \times 10^{-5}$ $B = 0.79$	$A = 8.0 \times 10^{-5}$ $B = 0.305$	$A = 8.0 \times 10^{-5}$ $B = 0.305$
In-cloud (rainout)	$A = 8.4 \times 10^{-5}$ $B = 0.79$	$A = 3.36 \times 10^{-4}$ $B = 0.79$	$A = 8.0 \times 10^{-5}$ $B = 0.305$	$A = 3.36 \times 10^{-}$ $B = 0.79$

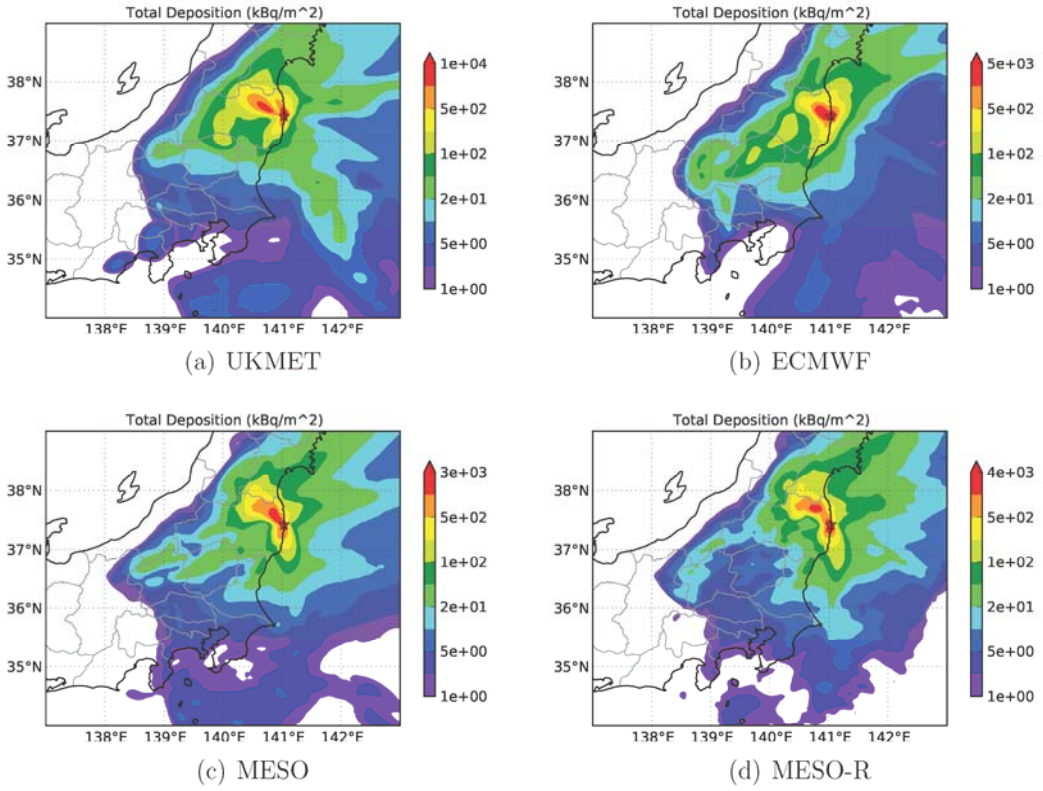

Fig. F-2-1. Deposition maps from NAME using 4 different meteorological data sets. UK (UKMET), European Centre (ECMWF), JMA Mesoscale (MESO) and JAM Mesoscale plus radar rainfall (MESO-R).

F-3. Impact of different meteorological input on ATM with FLEXPART[1]

F-3-1. Introduction and data

The work focuses on the influence of different meteorological input data (from JMA, ECMWF and NCEP), especially with regard to precipitation, on atmospheric transport modeling (ATM) simulations of aerosol-bound radionuclides with the Lagrangian particle dispersion model FLEXPART, version 8.23 (Stohl et al. 1998, 2005). Precipitation is known to be the most decisive factor for ground-level contamination (e.g. Clark and Smith, 1988) due to the efficiency of wet deposition processes (below-cloud and in-cloud scavenging). High resolution total precipitation fields from the operational Japanese Mesoscale analysis (~ 5 km horizontal resolution) and a radar-rain gauge analysis product (~ 1 km horizontal resolution) supplied by the JMA (JMA, 2012; Saito et al., 2015) offered a unique opportunity to assess the influence of spatially highly resolved precipitation input data in ATM for the particular case of the Fukushima Dai-ichi accident. In a pragmatic, yet limited, approach the latter fields were used to replace precipitation in the global or regional ECMWF (~0.125° native resolution) and global NCEP (~0.5° native resolution) data (see http://www.ecmwf.int/research/ifsdocs/CY37r2/index.html and http://www.emc.ncep.noaa.gov/GFS/doc.php) bearing in mind that there may be inconsistencies between the wind and precipitation fields. However, as precipitation is often not well modeled by NWP models but of high importance for deposition it was felt that it was important to investigate the impact of this potential off-line method for improving the precipitation fields used in ATM. The publicly available gridded ^{137}Cs deposition map (USDOE, United States Department of Energy, 2011; MEXT, 2011c) for land in area surrounding the Fukushima NPP and ^{137}Cs air concentration measurements from the International Monitoring System (IMS) of CTBTO were used for verification. For this study the ^{137}Cs source term by Terada et al. (2012) was used.

F-3-2. Atmospheric transport modeling

FLEXPART version 8.23 (which differentiates between in-cloud and below-cloud scavenging) includes a disadvantage that needs to be tackled. This disadvantage consists of the fact that clouds are diagnosed according to the exceedance of 80% relative humidity and that values are interpolated spatially and temporally using nearest neighbor interpolation. Thus, a particle may encounter precipitation, where no cloud is present, which leads to zero wet deposition for this grid point, a problem which is especially relevant for convective clouds/precipitation. A fix to this problem was proposed by Seibert et al. (2012) and tested within this evaluation. It includes a stepwise reduction of the relative humidity threshold (from 90% down to 25%) for diagnosing clouds if precipitation is present. Cloud base and height are interpolated from surrounding grid points in time and in space. If no clouds can be found there and precipitation is present the previous bulk parameterization for in cloud and below cloud scavenging is used.

---

[1] C. Maurer, D. Arnold and G. Wotawa

In line with Draxler and Heffter (1981) and as described in Draxler et al (2013a), independent forward runs with a unit source emission rate for 3 hourly release periods were performed every 3 hours to yield the source-receptor sensitivities for each release segment. These runs were finally scaled by the source strength in the corresponding release segment and summed up to give the actual modeled values at each time step and grid point. Following Draxler (2006) the statistical parameters correlation (R), fractional bias (FB), figure-of-merit in space (FMS) and the Klomogorov-Smirnov parameter (KSP) were used individually and in combination in a single measure called RANK (ranging from 0, worst, to 4, best) to quantitatively assess the model performance of the local runs.

F-3-3. Results

A summary of results can be found in **Table F-3-1**.

a. NCEP-0.5° versus ECMWF-0.5°

The differences between NCEP-0.5° and ECMWF-0.5° (abbreviated in **Table F-3-1** as NC-0.5 and EC-0.5) are worth mentioning. Maxima for the EC-0.5 driven run are around five times larger than for NC-0.5. The overall deposition is larger for EC-0.5 and the measured maximum with depositions over 500 kBqm^{-2} to the Northwest of the power plant is clearly better represented using ECMWF input data (**Fig. F-3-1**). All statistical scores mentioned above (**Table F-3-1**) as well as a scatter diagram (not shown) confirm the view that the ECMWF run ranks better than the NCEP run.

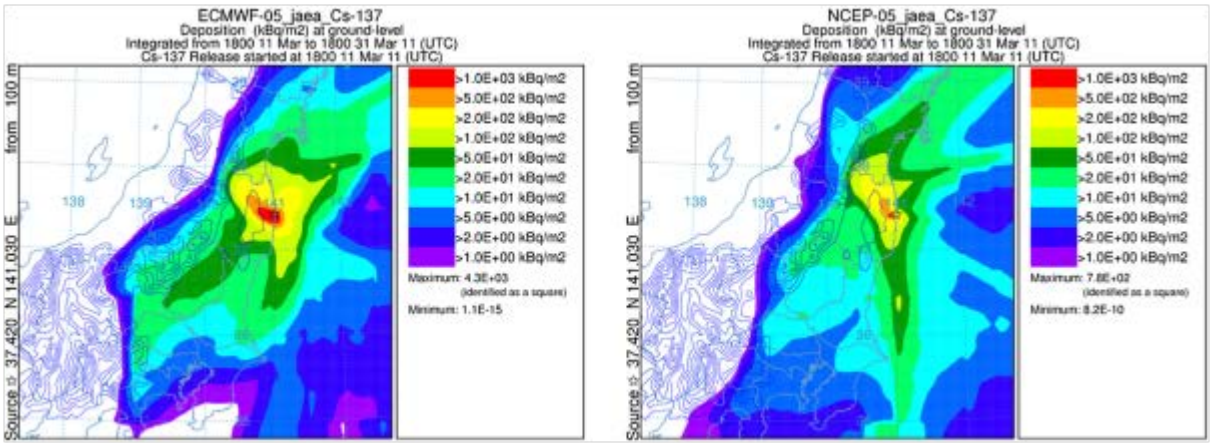

Fig. F-3-1.: Total accumulated deposition running FLEXPART with ECMWF (left) and NCEP (right) data both at 0.5° horizontal resolution. From Arnold et al. (2015), Fig.3.

b. ECMWF-0.2/0.1° versus ECMWF-0.5°

Increasing the horizontal resolution in the ECMWF fields used in the dispersion simulations from 0.5° to 0.2° (runs EC-0.2 and EC-0.5° in **Table F-3-1**) leads to the expected increase in structure and a more realistic appearance (**Fig. F-3-2**). The lower resolution input results in a smoother deposition field and larger area covered with smaller values in the plume axis northwest of Fukushima. Another important outcome is the increased deposition on the slope of the mountain district of Northern Japan as well west of the Kanto plain. This increase is carried forward if the resolution in the ECMWF field

gets enhanced to 0.1° (**Fig. F-3-2**). Performance metrics showed some slight improvements with the increase in horizontal resolution from 0.5° to 0.2°. However, using 0.1° input data lessens the Rank, which fits many experiences for model-to-point comparisons, where with increasing resolution of the meteorological input small dislocations between modeled patterns and measurements increasingly deteriorate statistical scores. Nevertheless it is advisable to use input data of 0.2° instead of 0.5° for ATM applications.

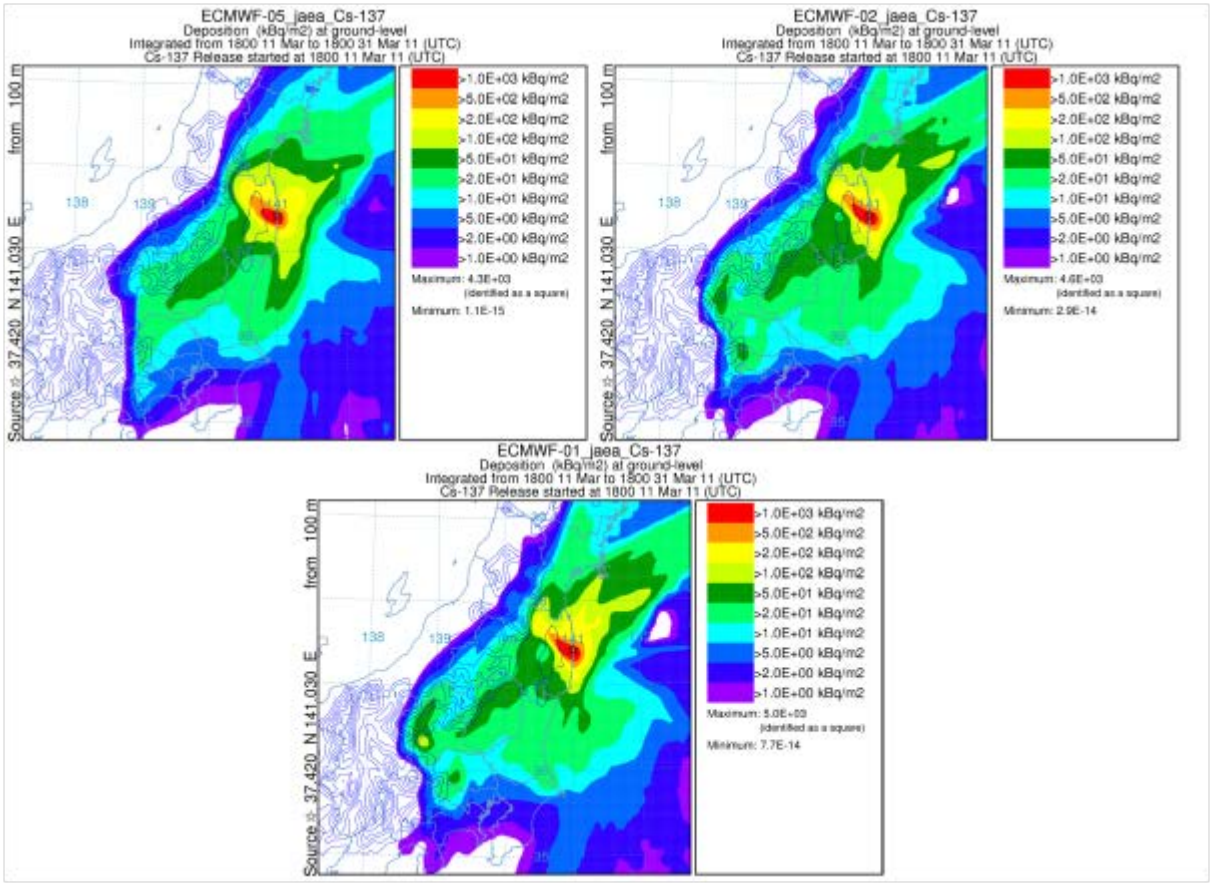

Fig. F-3-2.: Total accumulated deposition running FLEXPART with ECMWF at 0.5° (left), 0.2° (right) and 0.1° (center) horizontal resolution. Partly from Arnold et al. (2015), Fig.5.

c. ECMWF-0.2° versus ECMWF-0.2° with inserted JMA products

When replacing model precipitation with the radar-rain gauge analysis data in the 0.2°-ECMWF fields (ECRA-0.2 run in **Table F-3-1**) scores worsen slightly, whereas they improve when ingesting the Mesoscale precipitation analysis (ECME-0.2 run in **Table F-3-1**). In the first case the continuous maxima northwest of the NPP changes to a two-maxima pattern (**Fig. F-3-3**), in the second case the area with the greatest deposition extends a bit further north, thereby matching better the measurements. The regions with lower deposition to the south-west are also better represented. Maximum values turn out to be larger in both cases compared to plain ECMWF input data. The ingestion procedure was also applied to NCEP data, but resulted in a general worsening of results for both kinds of JMA-precipitation data (see results for NCME-0.5 and NCRA-0.5 in **Table F-3-1**). In this case the

elongated maximum to the northwest of the NPP is not reproduced. The results indicate an inconsistency between NCEP wind fields and observed precipitation, which in turn hints at a weaker performance of NCEP wind fields compared to those from ECMWF.

When the above described fix for wet deposition is applied to the FLEXPART source code, modeled depositions tend to worsen for plain ECMWF input data (regardless of the resolution) by 2-3% (see **Table F-3-1**). For example, the main deposition area becomes overestimated by the EC-0.2MC run, deposition onshore and inland towards the south also exceed the observations. Contrariwise, the runs with the ingested JMA-products (ECME-0.2MC and ECRA-0.2MC) show ranks improved by 2.3 and 5% respectively, mainly due to enhanced scavenging to the northwest of the NPP. It looks as if the consistency between precipitation fields and other meteorological input data, which is questionable in case of the ingestion of JMA precipitation products, is more important for the currently applied deposition scheme in FLEXPART version 8.23. This becomes understandable when one bears in mind that wet deposition for a grid point is only activated in this scheme if a cloud is diagnosed from relative humidity. With independent precipitation data the scheme is even more problematic than with dependent one.

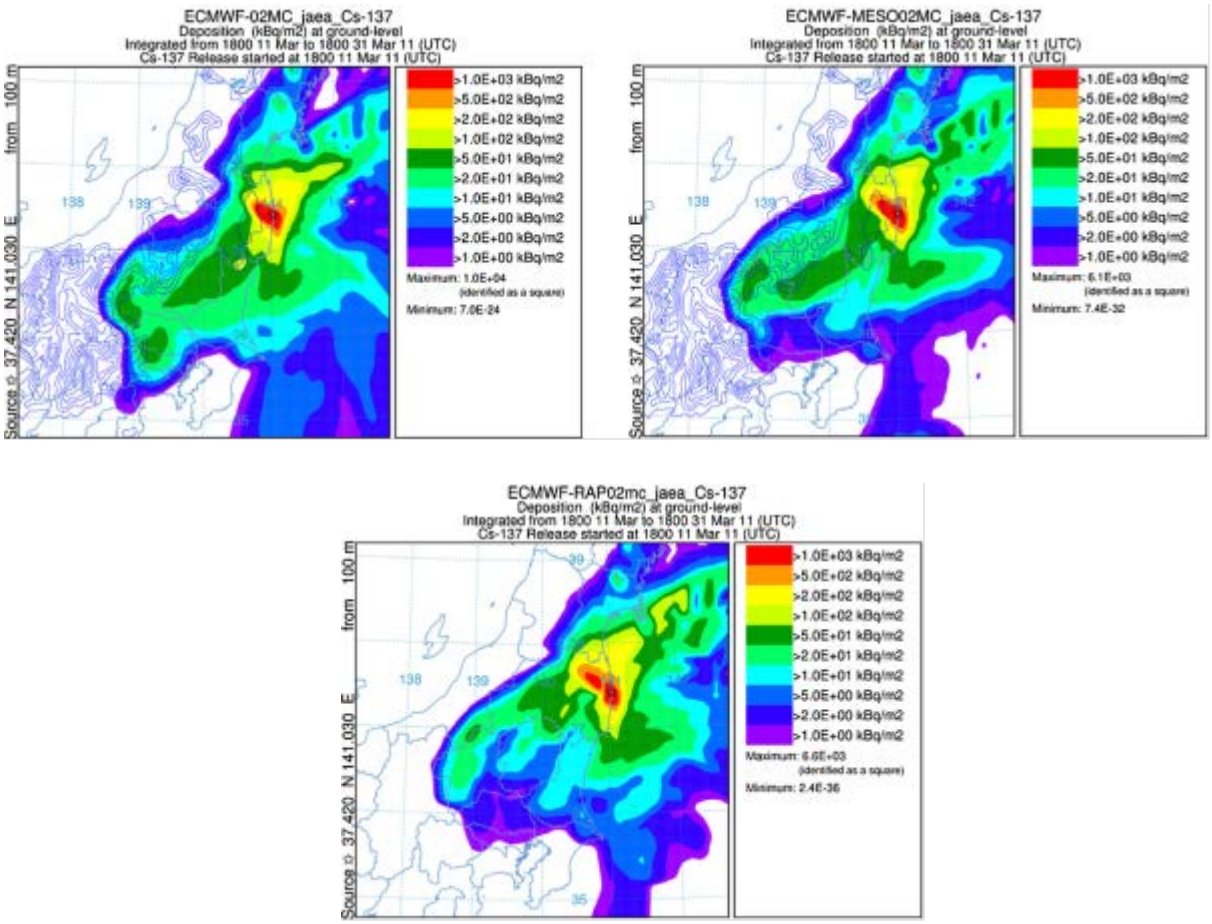

Fig. F-3-3.: Deposition patterns obtained with the quick fix for the wet deposition scheme in FLEXPART for the EC-0.2MC (upper left), the ECME-0.2MC (right) and the ECRA-0.2MC (center) runs.

Name	Met. precip. info.	Resolution (deg)	Corr	FB	FMS	KSP	Rank
EC-0.2	ECMWF	0.2	0.80	−0.08	100.00	15.00	3.44
EC-0.2MC	ECMWF	0.2	0.69	0.08	100.00	7.00	3.36
EC-0.5	ECMWF	0.5	0.71	−0.07	100.00	9.00	3.38
EC-0.5MC	ECMWF	0.5	0.68	0.09	97.24	10.00	3.28
ECRA-0.2	ECMWF + RAP	0.2	0.72	0.02	100.00	11.00	3.39
ECRA-0.2MC	ECMWF + RAP	0.2	0.83	0.13	100.00	6.00	3.57
ECME-0.2	ECMWF + MESO	0.2	0.81	0.00	100.00	15.00	3.50
ECME-0.2MC	ECMWF + MESO	0.2	0.83	0.05	100.00	9.00	3.58
NC-0.5	NCEP	0.2	0.66	−0.59	100.00	10.00	3.05
NCME-0.5	NCEP + MESO	0.5	0.65	−0.76	100.00	16.00	2.88
NCRA-0.5	NCEP + RAP	0.5	0.66	−0.84	100.00	20.00	2.82

Table F-3-1.: Statistical scores for the individual FLEXPART runs with different meteorological input data. MC label indicates the wet deposition FLEXPART quick fix was implemented. From Arnold et al. (2015), Fig.8 and Table 2.

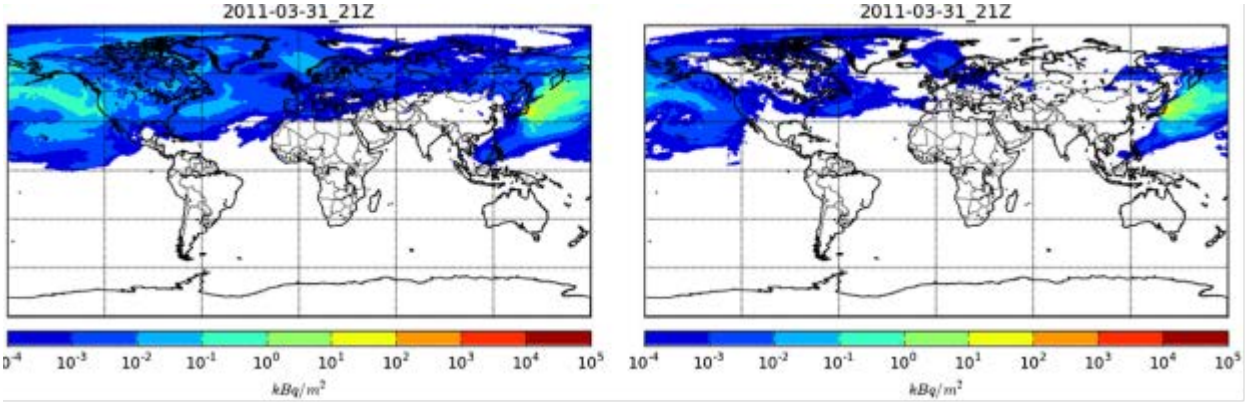

Fig. F-3-4.: Total global deposition on the 31st of March at 21 UTC for NCEP driven run (left) and ECMWF driven run (right). From Arnold et al. (2015), Fig.10.

d. Hemispheric run

Finally two hemispheric runs were evaluated with releases being tracked until the 31st of March. The runs were driven by global 0.5°-ECMWF data with a 0.2° nest (ECME-0.2 data) over Japan and by global 0.5°-NCEP data. Modeled ^{137}Cs depositions (**Fig. F-3-4**, however not comparable to any measurements) as well as ambient air concentrations (**Fig. F-3-5**) are generally higher using NCEP data as input. The plume arrival time and the two maxima pattern are quite well reproduced by FLEXPART at the IMS stations USP78 and USP79 (both located in the Central Pacific) both for ECMWF and NCEP input data. However, for ECMWF input the simulated concentrations are clearly underestimated, reaching up to a difference of two orders of magnitude. Overall uncertainties in patterns and magnitudes grow with increasing distance to the release location.

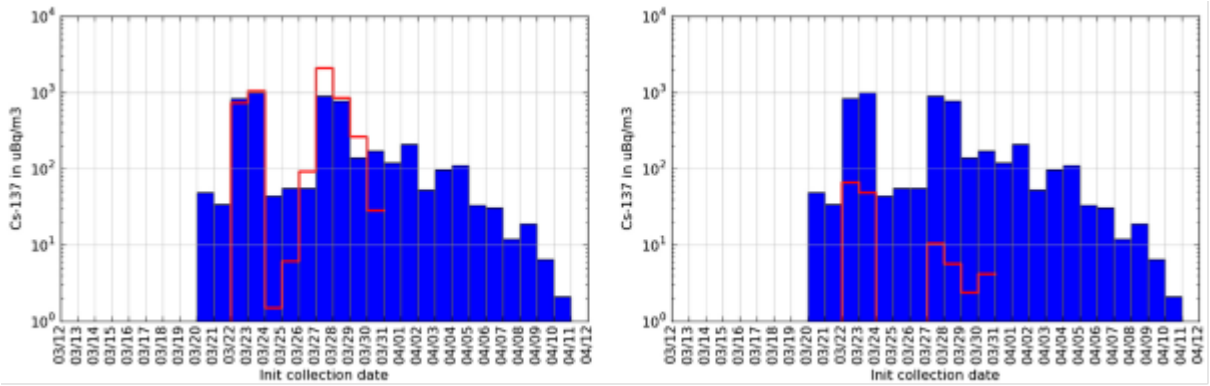

Fig. F-3-5: Time series of ^{137}Cs concentration at the USP78 IMS station. Measurements (blue) compared to modeled (red) concentrations with NCEP (left) and ECMWF (right) data. From Arnold et al. (2015), Fig.11.

F-3-4. Summary

The local model performance is clearly superior for 0.5° ECMWF fields compared to 0.5° NCEP fields given the Fukushima accident and the specific source term due to a systematic underestimation in NCEP results. Increasing the resolution from 0.5° to 0.2° for the ECMWF data seems beneficial. Inserting the Japanese Mesoscale precipitation analysis in 0.2°-ECMWF fields yielded the best result, especially when a wet deposition fix was applied. For the radar-gauge product things are different. They lead to a worsening in deposition when no fix is applied and to a bettering if it is applied, since the fix makes the model more robust to inconsistencies between wind and precipitation fields. Hemispheric runs yield more realistic concentration amplitudes (see Arnold et al. (2015) for more results) if driven by NCEP data.

F-4. The CMC ATDM experiments[1]

MLDP0 (*Modèle Lagrangien de Dispersion de Particules d'ordre 0*) is a Lagrangian particle dispersion model of zeroth order designed for long-range dispersion problems occurring at regional and global scales and is described in details in D'Amours and Malo (2004) and D'Amours et al. (2010). Dispersion is estimated by calculating the trajectories of a very large number of air particles (also called parcels or fluid elements). Large scale transport is described by calculating the displacement due to the synoptic component of the wind field and diffusion through discretized stochastic differential equations to account for the unresolved turbulent motions. Vertical mixing caused by turbulence is handled through a random displacement equation (RDE) based on a diffusion coefficient K_z. The calculation of the diffusion coefficient combines two formulations following Delage (1997), for the surface layer, and O'Brien (1970), for the above layers, in order to produce a vertical profile of K_z consistent with the depth of the ABL (due to the reflection condition at the top of the ABL). This coefficient is calculated in terms of a mixing length, stability function, and vertical wind shear. Lateral mixing (horizontal diffusion) is modelled according to a first order Langevin Stochastic Equation for the unresolved components of the horizontal wind (mesoscale fluctuations).

MLDP0 is an off-line model that uses the full 3-D meteorological fields provided by a numerical weather prediction (NWP) system, i.e. fields of wind, moisture, temperature and geopotential heights must be provided to the model. These are normally obtained from the GEM model forecasts and objective analysis systems in either global, regional or high resolution configuration.

In MLDP0 a computational particle (or parcel) is assumed to represent the ensemble average of a large number of "real" air constituents (aerosols or gases). At the emission, it is assigned a mass which depends on the total quantity of material emitted and the total number of particles. The effect of radioactive decay, wet scavenging, dry deposition and gravitational settling can be simulated by calculating the amount of material removed from the carrier particle, when it travels in regions of the atmosphere where such processes are active.

Dry deposition occurs when a particle is subjected to a reflection at the ground surface. It is modelled in terms of a dry deposition velocity v_d and an absorption probability P. The absorption probability is calculated according to Wilson et al. (1989) as

$$P = 1 - R\,, \quad R = \frac{1-a}{1+a}\,, \quad a = \left(\frac{\pi}{2}\right)^{1/2} \frac{v_d}{\sigma_w}\,, \tag{F-4-1}$$

[1] A. Malo and R. Servranckx

where R is the reflection probability and σ_w is the standard deviation of the vertical turbulent wind component. Since a particle represents the mean of an ensemble of particles, the fraction of the mass removed by dry deposition is equal to P. The deposition rate is calculated by assuming that a particle contributes to the total surface deposition flux in proportion to the tracer material it carries when it is found in a layer adjacent to the ground surface. Dry deposition increment dm_d for particle p over a model time step dt can be expressed as

$$dm_d = P \cdot m_p = (1 - R) \cdot m_p \,, \tag{F-4-2}$$

where m_p is the particle mass. The new particle mass m'_p is then adjusted accordingly

$$m'_p = R \cdot m_p \,. \tag{F-4-3}$$

Wet deposition is treated with a simple scheme and will occur when a particle is presumed to be in a cloud (*in-cloud scavenging*) and is modelled in terms of a wet scavenging rate. Below-cloud scavenging is not considered yet in the operational version of MLDP0. The tracer removal rate is proportional to the local cloud fraction f_c and the particle mass m_p. Wet deposition increment dm_w for particle p over a model time step dt and updated particle mass are calculated using the following relationships

$$dm_w = m_p \cdot \left[1 - \exp(-s_w f_c dt)\right], \tag{F-4-4}$$

$$m'_p = m_p \cdot \exp(-s_w f_c dt), \tag{F-4-5}$$

where s_w is the wet scavenging rate (s^{-1}). Local cloud fraction is parameterized according to Pudykiewicz (1989) as a function of relative humidity following

$$f_c = \frac{U - U_t}{U_s - U_t}, \quad \text{if } U \geq U_t \,, \tag{F-4-6}$$

where f_c is the cloud fraction, U is the relative humidity, U_t is the threshold value of the relative humidity above which the subgrid scale condensation occurs (75% is the default value in MLDP0), U_s is the relative humidity for the saturation state (100%). Local cloud fraction can be estimated in both hindcast and forecast modes, using analysed and forecast NWP meteorological fields.

Gravitational settling in the trajectory calculations is computed according to Stokes' law for fine particles. By default, MLDP0 is run neglecting gravitational settling effects. However, this optional removal process can be included accounting together for a particle size distribution and density of a particle. This process represents an important removal mechanism in atmospheric transport modelling and can modify significantly modelled airborne concentrations and total ground deposition at short scale (near the source) as well as at very long range. This impact is related especially to the particle size

distribution used in the modelling. In order to properly model this physical process, it is therefore necessary to have a good knowledge of particle size distribution, something that is rarely known or available.

In MLDP0, tracer concentrations at a given time and location are obtained by assuming that particles carry a certain amount of tracer material. The concentrations are then obtained by calculating the average residence time of the particles, during a given time period, within a given sampling volume, and weighting it according to the material amount carried by the particle. Concentrations can be estimated more accurately close to the source with a Lagrangian model as compared to an Eulerian model. It is important to note that in MLDP0, all concentrations are averaged in space and time. The concentrations are averaged in the vertical layers and in the horizontal (surrounding grid points weighting algorithm) for smoothing effects and artificial noise attenuation as well as over the output time period/step/resolution specified by the modeller. For example, concentration outputs at 3-h time steps would correspond to average values over that 3-h period.

Three generic species were modelled as surrogates for the radionuclides: a gas with no wet or dry scavenging to mimic noble gases (such as ^{133}Xe), a gas with a relatively large dry deposition velocity (1 cm/s) and wet removal rate (3×10^{-4} s^{-1}) to represent a depositing gas (such as gaseous ^{131}I), and a particle with a small dry deposition velocity (0.1 cm/s) and wet scavenging rate (3×10^{-5} s^{-1}) to represent light particles (such as ^{137}Cs or particulate ^{131}I). Details are shown in Table F-4-1.

Table F-4-1. Different physical removal processes accounted in MLDP0 simulations (Draxler et al., 2013a).

Type	Species Name	v_d [cm/s]	s_w [s^{-1}]	Dry Deposition	Wet Scavenging	Radioactive Decay	Gravitational Settling	Surrogate for
Gas	Ngas	0	0	No	No	No	No	Noble gases (Kr, Xe, Rn)
Particle, light	Lpar	0.1	3×10^{-5}	Yes	Yes	No	No	^{137}Cs, ^{131}I
Gas, depositing	Dgas	1	3×10^{-4}	Yes	Yes	No	No	^{131}I

F-5. Results of ATDM simulations[1]

F-5-1. ATDM simulations using UNSCEAR source term

The ATDM simulation results from the task team are summarized in WMO (2012b) and Draxler et al. (2013a). The experiments were conducted according to the experimental design protocol described in D-1.

Figure F-5-1 shows a sample of the calculated ^{137}Cs deposition patterns from NOAA-HYSPLIT (top) and UKMET-NAME (bottom) using the UNSCEAR source term. Here, the left panels show the predicted deposition patterns using the ECMWF meteorology, while the right panels show the model results using the JMA MESO meteorology. The UKMET results tend to be smoother than the NOAA calculation which is especially striking for the calculations using the finer resolution MESO data.

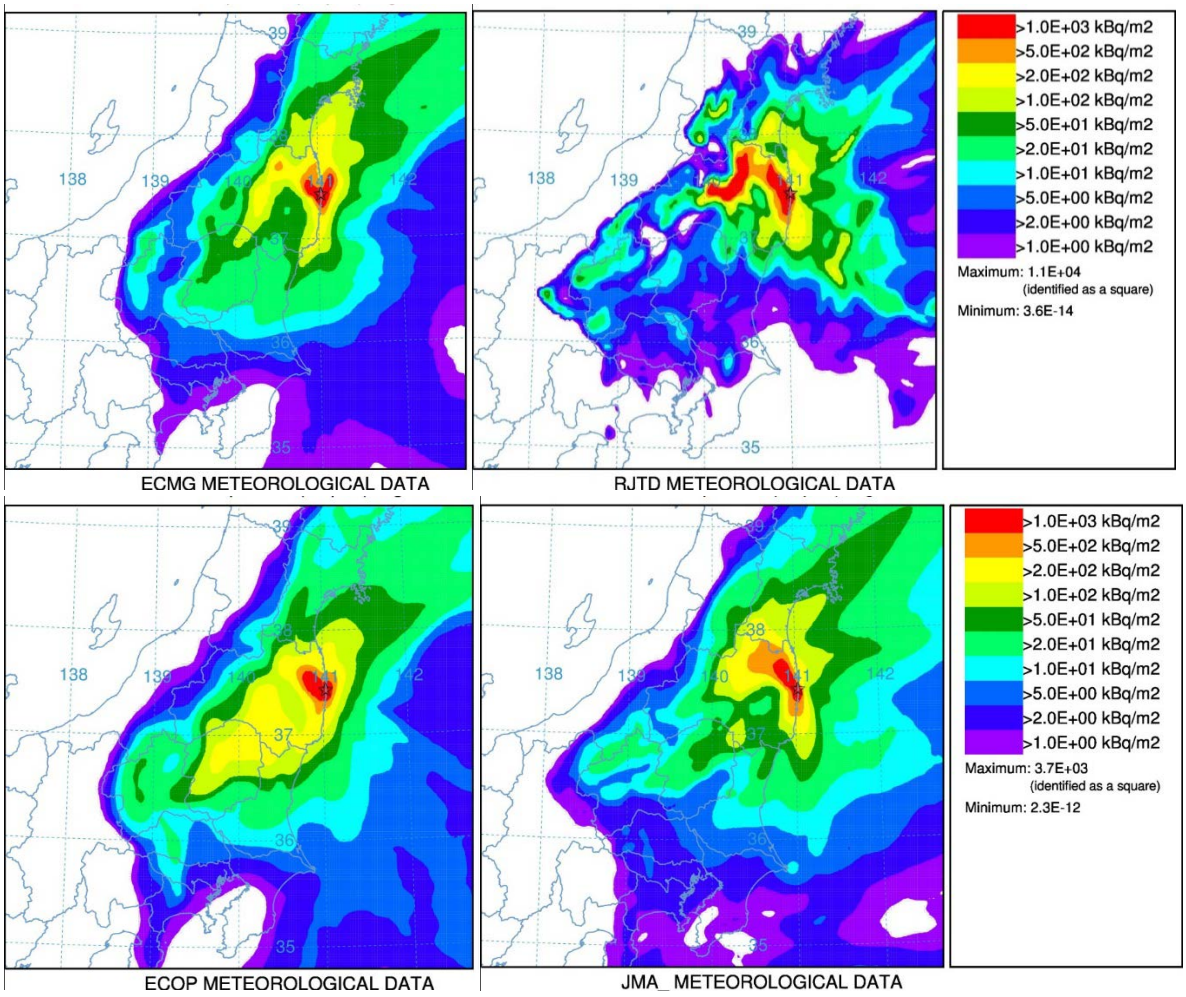

Fig. F-5-1. Upper: Calculated ^{137}Cs deposition using NOAA-HYSPLIT ATDM with ECMWF data (left) and with the JMA-MESO analysis (right). Bottom: UKMET-NAME ATDM with ECMWF data (Left) and with the JMA-MESO analysis (right). Reproduced from Draxler et al. (2013a).

[1] K. Saito, R. Draxler, T. Shimbori, M. Hort, G. Wotawa, A. Malo and R. Servranckx

An example of the computed ^{137}Cs deposition pattern for the ensemble mean of ten selected members (Draxler et al., 2013a) from all task tem ATDMs is shown in Fig. F-5-2. The computed high deposition region shows a comparable downwind direction to the measurements (Fig. D-3-1), including the turn to the southwest, less transport to the north, and a much smoother pattern, more consistent with the measurements.

Detailed verification results for the case using UNSCEAR source term is given in Draxler et al. (2013a).

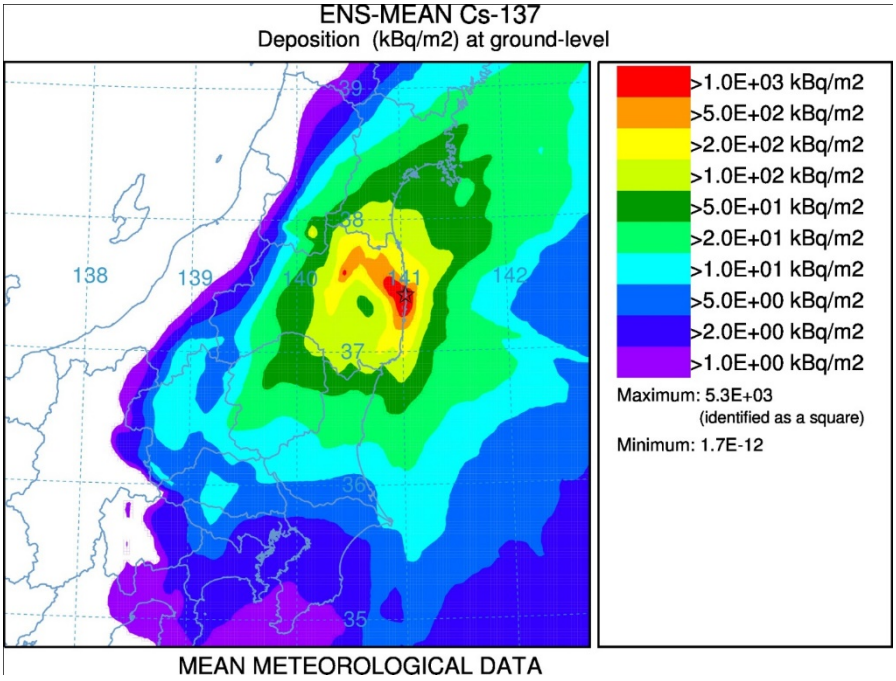

Fig. F-5-2. Calculated ^{137}Cs deposition using the mean of ten selected ATDM-meteorology combinations. After Draxler et al. (2013a).

F-5-2. Verification results using JAEA source term

The results of ATDM simulations and their verifications have been published in WMO (2012b) and Draxler et al. (2013a). In this subsection, verification results using JAEA source term are briefly summarized from the above publications.

Table F-5-1 shows ATDM verification results for ^{137}Cs deposition using JAEA source term. In this table, JMA (PRE) shows the results from the preliminary JMA-RATM simulations before the modifications described in Section E-2 were applied. METRIC1 is the total model rank defined by the Eq. (D-3-1). Here, the value of METRIC1 is positive and becomes 4.0 for a perfect case. For ^{137}Cs deposition, NOAA-HYSPLIT using GDAS showed the best score for METRIC1. ZAMG-FLEXPART and, NOAA-HYSPLIT using ECMWF analysis and, UKMET-NAME using JMA-MESO also scored a relatively high performance. In NOAA-HYSPLIT, the use of JMA MESO analysis did not improve

the METRIC1, while the results of CMC-MLDP0 and UKMET-NAME were improved by the use of JMA MESO.

Table F-5-2 shows ATDM verification results for air concentrations at JAEA. Including the best score by CMC and the second best by JMA-RATM, all the top five ranked models used the JMA Meso analysis for their computations.

Replacing the JMA Mesoscale analysis precipitation fields with JMA precipitation observation analysis (MESO-R) did not improve the ATM calculations of deposition and even deteriorated the scores for air concentration. The reason for this is not clear. It should be noted that the air concentration verification was for a single location (JAEA) thus it does not reflect the horizontal distribution of radionuclides. The southward advection of radionuclides from Fukushima Daiichi NPP on March 15th was sensitive to small changes in the wind direction. As for deposition, ZAMG-FLXPART using ECMWF analysis slightly improved its score when the precipitation analysis was used. Saito et al. (2015) suggested the following reasons that the precipitation analysis did not improve the performance of ATM calculations:

The discrepancy of the transport patterns created using numerical weather prediction (NWP) analyses and the locations of the actual precipitation may result in a wrong description of the total wet scavenging. The quality of the RAP data itself is also arguable. Although the bright band (shown in Fig. B-3-2) is not likely critical in this experiment, radar echoes are scanned around the level of 1 km AGL and solid waters are over-detected in the radar reflectivity. A lower detection limit of around 0.4 mm h^{-1} applies to the RAP, which means that very weak precipitation is not included. In case of JMA-RATM, all RAP precipitation was considered to be liquid rain in the wet scavenging calculation (see Section E-2), and this assumption also may yield some errors in the time evolution.

Table F-5-1. ATDM verification results for ^{137}Cs deposition using JAEA source term. First to fifth values of METRIC1 are indicated by bold type. In analysis, '-R' means that JMA precipitation analysis is used. Reproduced from Draxler et al. (2013a).

Organization	Analysis	R	FB	FMS	FOEX	%FA2	KSP	METRIC1
CMC	GEM	0.76	-0.32	100.00	11.69	48.99	19.00	3.22
CMC	MESO	0.76	-0.44	100.00	-4.33	45.12	6.00	3.30
JMA (PRE)	MESO	0.45	-0.02	100.00	-0.46	51.01	10.00	3.09
JMA (PRE)	MESO-R	0.77	0.54	100.00	9.67	41.99	11.00	3.22
NOAA	GDAS	0.87	-0.08	100.00	8.01	48.25	6.00	**3.65**
NOAA	GDAS-R	0.68	-0.57	100.00	-16.48	31.86	23.00	2.94
NOAA	MESO	0.55	0.38	100.00	-8.01	41.07	15.00	2.97
NOAA	MESO-R	0.48	0.43	100.00	-4.14	35.54	16.00	2.85
NOAA	ECMWF	0.83	-0.30	100.00	-12.06	46.96	10.00	**3.45**
NOAA	ECMWF-R	0.55	-0.74	100.00	-20.35	21.92	33.00	2.60
UKMET	UM	0.44	0.24	100.00	30.48	42.36	30.00	2.77
UKMET	ECMWF	0.80	0.11	100.00	19.06	54.70	25.00	3.34
UKMET	MESO	0.76	0.04	100.00	5.80	45.12	11.00	**3.45**
UKMET	MESO-R	0.66	0.03	100.00	6.35	34.62	9.00	3.33
ZAMG	GDAS	0.66	-0.59	100.00	-6.17	45.12	10.00	3.05
ZAMG	GDAS-R	0.66	-0.84	100.00	-16.85	28.36	20.00	2.82
ZAMG	ECMWF	0.78	-0.08	100.00	9.85	59.67	15.00	**3.41**
ZAMG	ECMWF-R	0.83	0.13	100.00	5.99	52.12	6.00	**3.57**

Table F-5-2. Same as in Table F-5-1, but for particulate ^{131}I air concentrations at JAEA. Reproduced from Draxler et al. (2013a).

Organization	Analysis	R	FB	FMS	FOEX	%FA2	KSP	METRIC1
CMC	GEM	0.07	-1.37	73.17	-30.95	7.14	53.00	1.52
CMC	MESO	0.23	-0.09	80.49	-4.76	16.67	34.00	**2.47**
JMA (PRE)	MESO	0.51	-0.82	80.00	-21.43	21.43	43.00	**2.22**
JMA (PRE)	MESO-R	0.59	-1.66	57.50	-45.24	4.76	64.00	1.46
NOAA	GDAS	0.10	-1.37	60.00	-42.86	7.14	69.00	1.24
NOAA	GDAS-R	0.10	-1.38	60.00	-42.86	7.14	67.00	1.25
NOAA	MESO	0.15	-1.63	62.50	-40.48	11.90	67.00	1.16
NOAA	MESO-R	0.15	-1.63	60.00	-40.48	9.52	67.00	1.14
NOAA	ECMWF	0.27	-1.33	62.50	-35.71	11.90	60.00	1.43
NOAA	ECMWF-R	0.27	-1.35	62.50	-35.71	16.67	60.00	1.43
UKMET	UM	0.06	-1.42	65.85	-30.95	19.05	53.00	1.42
UKMET	ECMWF	0.13	-0.93	68.29	-28.57	21.43	53.00	1.70
UKMET	MESO	0.24	-0.50	80.00	-28.57	16.67	52.00	**2.09**
UKMET	MESO-R	0.24	-0.53	80.00	-30.95	16.67	52.00	**2.07**
ZAMG	GDAS	0.17	-0.37	57.50	-35.71	14.29	57.00	**1.85**
ZAMG	GDAS-R	0.18	-0.43	57.50	-35.71	14.29	55.00	1.84
ZAMG	ECMWF	0.12	-0.54	52.50	-35.71	11.90	60.00	1.67
ZAMG	ECMWF-R	0.08	-0.55	42.50	-35.71	7.14	69.00	1.46